RNA sequencing-based approaches to identifying disulfidptosis-related diagnostic clusters and immune landscapes in osteoporosis

Peng Zhang[1], Bing Li[2], Honglin Chen[1], Zhilin Ge[1], Qi Shang[1], De Liang[3], Xiang Yu[3], Hui Ren[4], Xiaobing Jiang[4], Jianchao Cui[3]

[1]Guangzhou University of Chinese Medicine, Guangzhou 510405, China
[2]The First Affiliated Hospital of Guangxi University of Chinese Medicine, Nanning 530023, China
[3]The First Affiliated Hospital of Guangzhou University of Chinese Medicine, Guangzhou 510405, China
[4]The Second Affiliated Hospital of Guangzhou Medical University, Guangzhou 510260, China

Correspondence to: Hui Ren, Xiaobing Jiang, Jianchao Cui; **email:** renhuispine@163.com, https://orcid.org/0000-0003-1698-5505; spinedrjxb@sina.com, https://orcid.org/0000-0002-8009-0282; 149504193@qq.com, https://orcid.org/0000-0003-4358-1450

ABSTRACT

Disulfidptosis, a newly recognized cell death triggered by disulfide stress, has garnered attention for its potential role in osteoporosis (OP) pathogenesis. Although sulfide-related proteins are reported to regulate the balance of bone metabolism in OP, the precise involvement of disulfidptosis regulators remains elusive. Herein, leveraging the GSE56815 dataset, we conducted an analysis to delineate disulfidptosis-associated diagnostic clusters and immune landscapes in OP. Subsequently, vertebral bone tissues obtained from OP patients and controls were subjected to RNA sequencing (RNA-seq) for the validation of key disulfidptosis gene expression. Our analysis unveiled seven significant disulfidptosis regulators, including FLNA, ACTB, PRDX1, SLC7A11, NUBPL, OXSM, and RAC1, distinguishing OP samples from controls. Furthermore, employing a random forest model, we identified four diagnostic disulfidptosis regulators including FLNA, SLC7A11, NUBPL, and RAC1 potentially predictive of OP risk. A nomogram model integrating these four regulators was constructed and validated using the GSE35956 dataset, demonstrating promising utility in clinical decision-making, as affirmed by decision curve analysis. Subsequent consensus clustering analysis stratified OP samples into two different disulfidptosis subgroups (clusters A and B) using significant disulfidptosis regulators, with cluster B exhibiting higher disulfidptosis scores and implicating monocyte immunity, closely linked to osteoclastogenesis. Notably, RNA-seq analysis corroborated the expression patterns of two disulfidptosis modulators, PRDX1 and OXSM, consistent with bioinformatics predictions. Collectively, our study sheds light on disulfidptosis patterns, offering potential markers and immunotherapeutic avenues for future OP management.

INTRODUCTION

Osteoporosis (OP), as a prevalent skeletal disorder, is featured with loss of bone mass and structural alterations, rendering bones more susceptible to fractures and associated complications, such as pain, deformity, and heightened mortality risk [1–3]. Postmenopausal women, accounting for approximately 50% of individuals, are particularly vulnerable to OP-related fractures [4]. Current therapeutic strategies encompass a spectrum of interventions, including calcium, vitamin D, teriparatide, denosumab, and bisphosphonates [5]; however, prolonged administration of these agents may precipitate adverse reactions, including accelerated bone loss and heightened susceptibility to jaw osteonecrosis, femur fractures, and multiple vertebral fractures experiencing recompression [6]. Consequently, effective clinical management of OP

remains elusive [7], posing substantial challenges to healthcare systems and society at large [8]. Given the detrimental impact of OP on health, quality of life, and economic burden, early identification of high-risk individuals assumes paramount importance. Mounting evidence underscores the multifaceted nature of OP, emphasized by its considerable heterogeneity and genetic variability [9]. Accordingly, early risk stratification guided by genetic predispositions holds considerable promise in augmenting OP control efforts.

Disulfidptosis, a recently discovered cell death resulted from disulfide stress, emerges particularly under conditions of glucose deprivation, wherein cells exhibiting heightened SLC7A11 expression and aberrant accumulation of disulfide and cystine components undergo rapid demise due to NADPH consumption-induced disulfide stress [10]. This distinctive mode of cell death implicates a myriad of disulfide-regulatory markers, including FLNA, FLNB, SLC7A11, ACTB, MYH9, SLC3A2, TLN1, OXSM, PRDX1, LRPPRC, NUBPL, RPN1, NCKAP1, NDUFS1, RAC1, WAVE2, NDUFA11, and GYS1 [10]. Prior investigations have underscored the potential of sulfide-regulatory biomarkers as viable targets for diagnosis and therapeutic intervention in OP [11]. Subsequent studies have elucidated the involvement of the sulfide quinone reductase-like gene in modulating osteoblast differentiation [12], while highlighting disulfide's suppressive effect on osteoclast differentiation via the NF-κB/NFATc1 signalling pathway, thereby mitigating inflammatory osteolysis [13]. Notably, the emergence of disulfidptosis-related ribophorin I (RPN1) is reported to be a therapeutic target and diagnostic biomarker for OP, particularly in the context of kaempferol intervention [14]. These collective findings prompt speculation on the pivotal role of disulfidptosis in the pathological progress of OP through the modulation of disulfide stress-related protein expression. Nevertheless, the precise contributions of disulfidptosis modulators to OP pathogenesis remain elusive.

Utilizing the GSE56815 dataset [15], we investigated the relevance of disulfidptosis regulators in delineating OP subtypes and identifying potential diagnostic biomarkers. A predictive model for OP susceptibility was devised, integrating seven putative disulfidptosis regulators (FLNA, ACTB, PRDX1, SLC7A11, NUBPL, OXSM, and RAC1), demonstrating utility in clinical practice. Validation of these disulfidptosis regulators was conducted via RNA sequencing (RNA-seq), confirming expression patterns consistent with bioinformatics predictions. Furthermore, our analysis unveiled two distinct disulfidptosis patterns, exhibiting significant associations with many immune cells like monocytes.

These findings underscore the potential of disulfidptosis patterns as diagnostic markers for OP, offering insights into tailored immunotherapeutic interventions. Methodological approaches employed in this study align with previous published literature [16–18]. The flow chart of research process is described in Figure 1.

MATERIALS AND METHODS

Sample data retrieval for OP analysis

Utilizing the GEO data repository (http://www.ncbi.nlm.nih.gov/geo/), we accessed data pertaining to monocytes extracted from whole blood specimens of OP patients. The search parameters encompassed terms such as 'osteoporosis', 'BMD', 'gene expression', and 'microarray'. Selection criteria included datasets comprising a minimum of 60 samples, with at least 30 cases each in the control and OP cohorts, alongside availability of downloadable series matrix files and raw data. Ultimately, we opted for the GSE56815 dataset [15]. Within this dataset, we have pinpointed 40 samples each in the OP and control groups deemed eligible for further analysis.

Data collection

The conversion of microarray probes into symbols was achieved in the R software (v4.1.2), utilizing the annotation package obtained from the Bioconductor website(http://bioconductor.org/). Subsequently, the dataset underwent quantile normalization to ensure uniformity across samples, comprising 40 control and 40 OP cases. Utilizing the Limma R package, distinct disulfidptosis regulators within the dataset were identified through comparative analysis between control and OP cohorts, employing significance cutoff of |$\log_2$ fold change (FC)| > 0 and $P < 0.05$ [19]. Furthermore, the clusterProfiler R package facilitated the enrichment analyses of GO and KEGG to investigate potential mechanisms of action associated with disulfidptosis regulators in OP.

Model establishment

In our investigation of OP occurrence, we devised two models of support vector machine (SVM) and random forest (RF) as testing frameworks, employing various methodologies including ROC curve, reverse cumulative residual distribution, and residual box plots [17]. The RandomForest package for R environments was utilized to construct the RF model, selecting putative disulfidptosis mediators based on significance scores (Mean Decrease Gini) [16]. For the SVM model, the parameter n denoted disulfidptosis gene number, with every data point depicted as a singular position

situated within an *n*-dimensional realm. Subsequently, an optimal hyperplane was identified to effectively segregate the OP and control groups [20]. Furthermore, we devised a nomogram signature utilizing the R plugin rms, facilitating OP prediction based on selected candidate disulfidptosis regulators. To validate our model, we employed the GSE35956 dataset [21], comprising 5 OP samples and 5 controls subjected to analysis. Calibration curves were adopted to gauge the alignment between prediction values and actual outcomes. Additionally, clinical impact curve was constructed through decision curve analysis (DCA), assessing the utility of model-based decisions in patient management [16].

Subtype classification

Utilizing consensus clustering with resampling, every element and its corresponding subgroup number were determined with validation confirming the cluster coherence [16]. The ConsensusClusterPlus package for R environments was employed to unveil different disulfidptosis subtypes according to significant disulfidptosis regulators [22].

GO enrichment analysis of DEGs

Employing the Limma package for R environments, we discerned differentially expressed genes (DEGs) between disulfidptosis clusters adopting adjusted $P < 0.05$ and $|\log_2 FC| > 0.5$ as thresholds. Subsequent GO enrichment analysis, performed by the R plugin clusterProfiler, elucidated the potential involvement of DEGs in OP pathogenesis [23].

Disulfidptosis score assessment

Disulfidptosis scores for individual samples were computed through principal component analysis (PCA) quantifying disulfidptosis patterns. The evaluative formula utilized for calculating the disulfidptosis score was disulfidptosis score = $PC1_i$, where PC1 represents principal component 1 and i denotes crucial disulfidptosis gene expression [24].
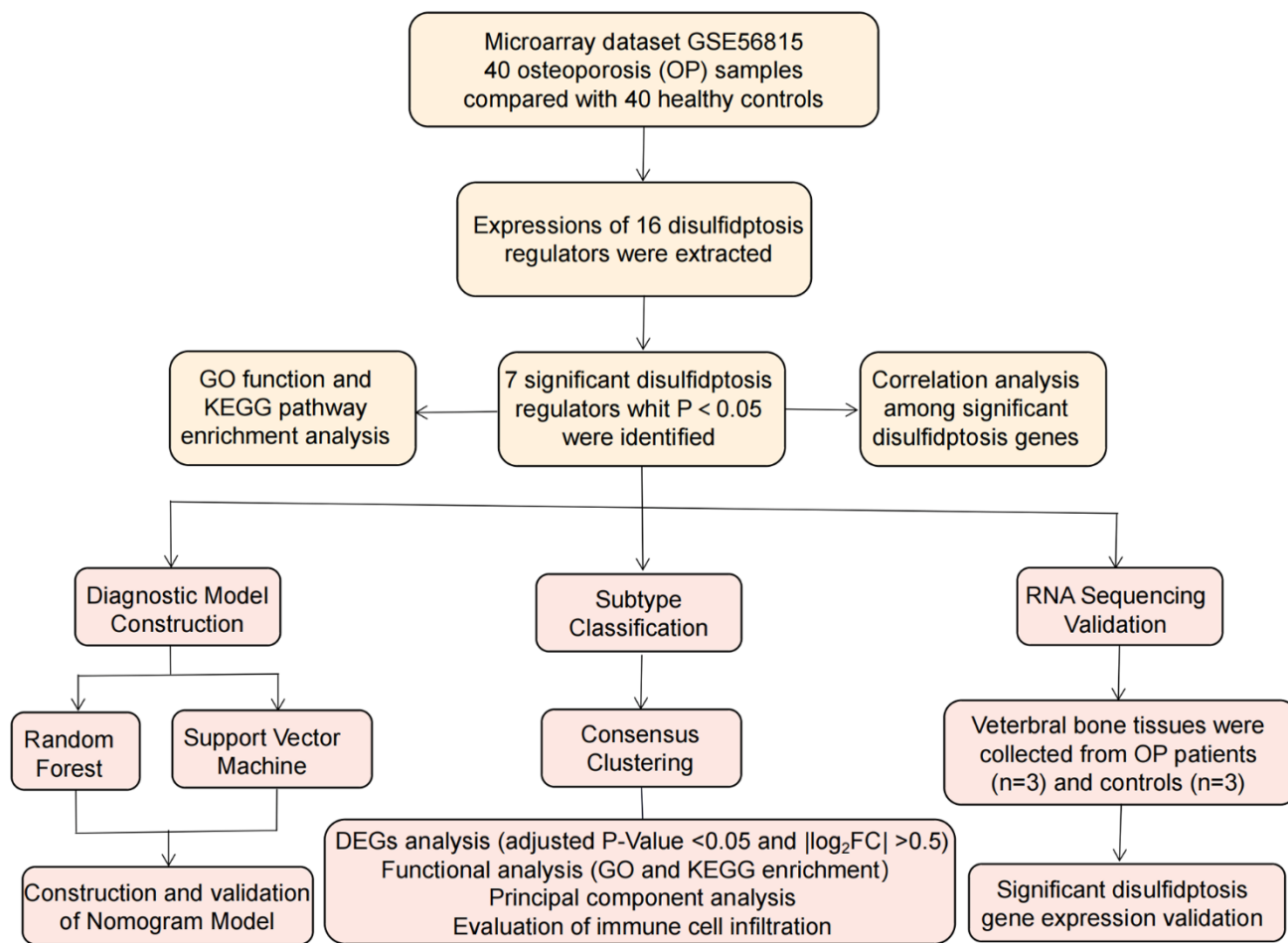

Figure 1. Flowchart of the study design.

Assessment of immune cell abundance

Immune cell infiltration in OP cases was evaluated via single-sample gene set enrichment analysis (ssGSEA). Initially, ssGSEA determined gene expression levels in samples, generating a ranking based on expression. Subsequently, the expression levels of key regulators of disulfidptosis were assessed, and their cumulative expression served to quantify immune cell populations within each sample [25].

RNA-seq analysis of vertebral bone samples from the OP and control groups to verify differential expression of disulfidptosis genes

Vertebral bone tissue samples were collected from individuals diagnosed with osteoporosis (OP) and control participants undergoing surgical treatment in the First Affiliated Hospital of Guangzhou University of Chinese Medicine. RNA-seq analysis was then employed to explore differential expressions of disulfidptosis-related genes between the two groups. Notably, no significant difference was noted in age, body mass index, serum phosphorus, serum alkaline phosphatase, and serum magnesium levels between the two groups. However, serum calcium levels, lumbar spine (L1–L4) T-score, and bone mineral density were significantly lower in the OP group in comparison to the control group ($P < 0.05$). Total RNA samples were collected from three OP patients and three control participants utilizing Trizol reagent. These RNA samples underwent agarose gel electrophoresis, Nanodrop quality inspection and quantification. The mRNA enrichment was performed using oligo magnetic beads, followed by library establishment for Illumina sequencing (Kapa Biosystems, Woburn, MA, USA). Library quality was evaluated, and quantification was conducted by quantitative polymerase chain reaction.

Subsequently, libraries from different samples were pooled based on quantitative results and final data for sequencing. DEGs in the dataset were screened by analyzing differences between control and OP samples adopting the Limma R package. Then, disulfidptosis modulators were identified and their expression profiles were constructed from the data. The screening thresholds used to detect disulfidptosis DEGs were set at $|\log_2 FC| > 1$ and $P < 0.05$.

Statistical analysis

The analysis of linear regression was utilized to assess the relationships between crucial disulfidptosis regulators. For bioinformatics analysis, group-wise comparisons were conducted using the Kruskal–Wallis test, while corrected t-tests were employed to analyze RNA-seq data. The parametric analysis was conducted using two-tailed tests, with statistical threshold set at $P < 0.05$.

RESULTS

Screening of 16 disulfidptosis regulators in OP

In total, 16 regulators associated with disulfidptosis were identified by analyzing gene expression profiles from both control and OP cases. From this analysis, seven distinct regulators (FLNA, ACTB, PRDX1, SLC7A11, NUBPL, OXSM, and RAC1) emerged, depicted in a heat map and box plot (Figure 2A, 2B). Notably, ACTB, FLNA, and NUBPL showed reduced expression levels, while PRDX1, SLC7A11, OXSM, and RAC1 exhibited increased expression in OP cases compared to controls (Figure 2C–2I). Additionally, GO analysis highlighted significant enrichment in biological process (tissue homeostasis), cellular components (glutamatergic synapses and actin filaments), and molecular function (L-glutamate transmembrane transporter activity) (Figure 2J). Furthermore, regulation of actin cytoskeleton and ferroptosis pathways emerged as the main enriched pathways according to KEGG analysis (Figure 2K). Detailed information regarding the GO and KEGG enrichment analyses can be found in Supplementary Tables 1, 2.

Correlations among disulfidptosis regulators in OP

In OP samples, there were significantly positive associations observed in the gene expressions of ACTB–FLNA, ACTB–RAC1, and PRDX1–OXSM (Figure 3A–3C). Conversely, significantly negative correlations were noted in the gene expressions of ACTB–SLC7A11, FLNA–SLC7A11, ACTB–OXSM, PRDX1–ACTB, RAC1–NUBPL, PRDX1–FLNA, and FLNA–OXSM (Figure 3D–3J). These observations underscore distinct correlations among various disulfidptosis modulators in OP.

Establishment of RF and SVM models

As depicted in Figure 4A, 4B, the RF model exhibited the smaller residuals, indicating its superior performance over the SVM model. Therefore, we utilized the RF model to forecast the occurrence of OP. ROC curve analysis revealed that the RF model outperformed the SVM model in terms of accuracy (Figure 4C). Consequently, we established an RF model to screen candidate disulfidptosis mediators for establishing a nomogram model [16]. Subsequently, the seven significant disulfidptosis regulators were ranked based on importance scores (mean decrease Gini), and four

regulators with scores > 6 (FLNA, SLC7A11, NUBPL, and RAC1) were selected as candidates (Figure 4D).

Nomogram model construction

We established a nomogram model utilizing the four nominated disulfidptosis regulators with the R plugin (rms) to forecast OP outcomes (Figure 5A). To validate this model, we utilized the GSE35956 dataset for further verification. The ROC analysis demonstrated notable AUC values, indicating a high level of diagnostic accuracy for this signature (Figure 5B). Additionally, the nomogram model exhibited favourable prediction accuracy as evidenced by calibration curves (Figure 5C). Notably, the DCA plot revealed that the red line continuously surpassed the black and gray lines across the entire probability range from 0 to 1, suggesting potential benefits for OP patients through decisions informed by the nomogram model (Figure 5D). Furthermore, the nomogram model displayed a reliable ability to predict outcomes, as demonstrated by Figure 5E.
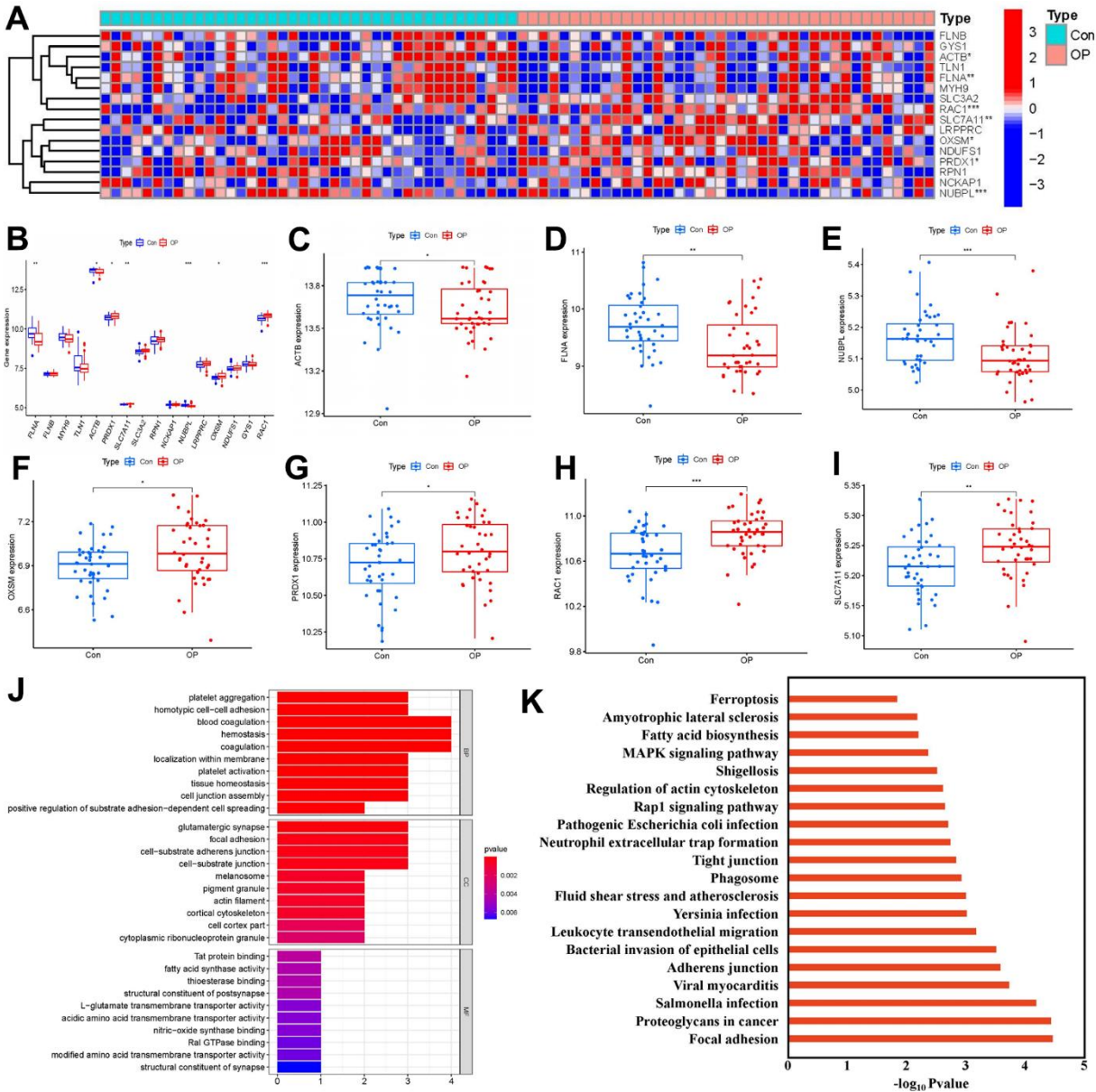

Figure 2. Identification of 16 disulfidptosis modulators in OP. (**A**) Expression heat map of 16 disulfidptosis modulators in OP cases and controls. (**B**) Differential expression box plot of 16 disulfidptosis modulators identified between OP cases and controls. (**C–I**) Differential expression box plots of seven significant disulfidptosis modulators identified between OP cases and controls. (**J**, **K**) GO and KEGG enrichment analysis based on seven significant disulfidptosis modulators. *$P < 0.05$, **$P < 0.01$, ***$P < 0.001$.
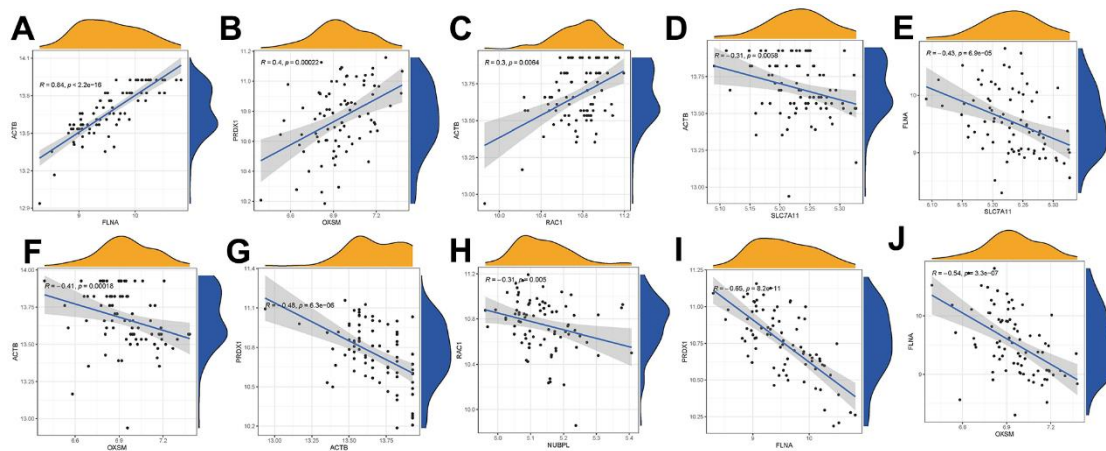
Figure 3. Correlations among disulfidptosis modulators in OP (**A–J**). In OP cases, there were significantly positive correlations in gene expression levels of ACTB–FLNA, ACTB–RAC1, and PRDX1–OXSM (**A–C**); there were significantly negative correlations in gene expression levels of ACTB–SLC7A11, FLNA–SLC7A11, ACTB–OXSM, PRDX1–ACTB, RAC1–NUBPL, PRDX1–FLNA, and FLNA–OXSM (**D–J**).
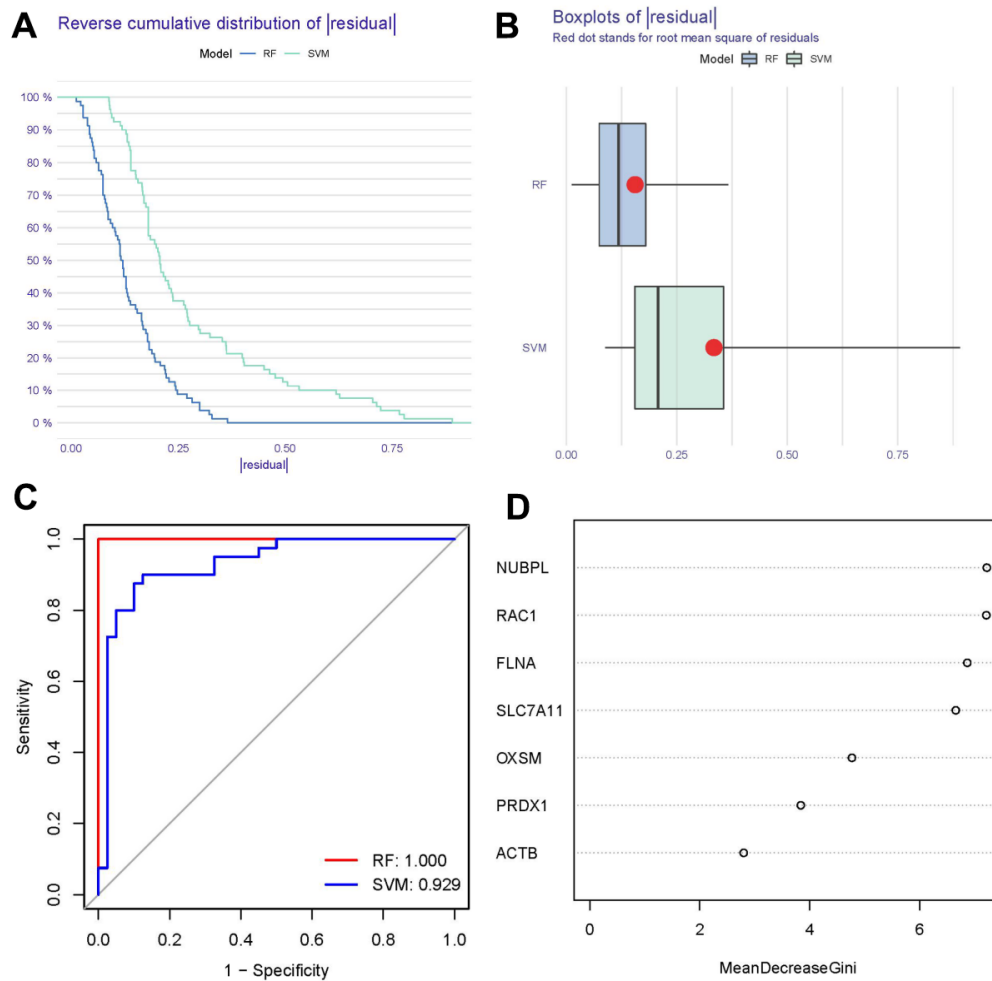

Figure 4. Establishment of RF and SVM models. (**A**) Reverse cumulative distribution constructed to display the residual distributions of RF and SVM models. (**B**) Box plot constructed to display the residual distributions of RF and SVM models. (**C**) ROC curves show the accuracies of the RF and SVM models. (**D**) Importance scores of seven disulfidptosis modulators based on the RF model.

Identification of two different disulfidptosis clusters

Through the utilization of ConsensusClusterPlus, we identified two distinct disulfidptosis clusters, denoted as clusters A and B, according to the expression profiles of the seven disulfidptosis regulators (Figure 6A–6D). Notably, cluster A encompassed 27 samples, while cluster B comprised 13 samples. Differential analysis of the gene expressions in the seven disulfidptosis modulators between these clusters revealed clear distinctions as depicted on heat maps and box plots. Specifically, cluster B demonstrated higher expression levels of FLNA, ACTB, and RAC1, whereas cluster A exhibited elevated expression levels of PRDX1 and OXSM. However, no significant differences were observed in the gene expressions of SLC7A11 and NUBPL between the two clusters (Figure 6E, 6F). PCA corroborated the discriminatory power of the seven disulfidptosis regulators in distinguishing between the two disulfidptosis clusters (Figure 6G). Subsequently, we identified 127 DEGs associated with disulfidptosis between the two clusters. To elucidate the functional roles of these DEGs in OP, we conducted GO enrichment analysis (Figure 6H), revealing enrichment terms such as regulation of actin cytoskeleton organization (GO: 0032956), regulation of actin filament-based process (GO: 0032970), cell-substrate junction (GO: 0030055), and actin binding (GO:0003779). The information containing the GO enrichment results was available in Supplementary Table 3.

Subsequently, we proceeded to investigate the associations between the seven pivotal disulfidptosis modulators and immune cells by utilizing ssGSEA to measure the abundance of immune cells in OP samples.
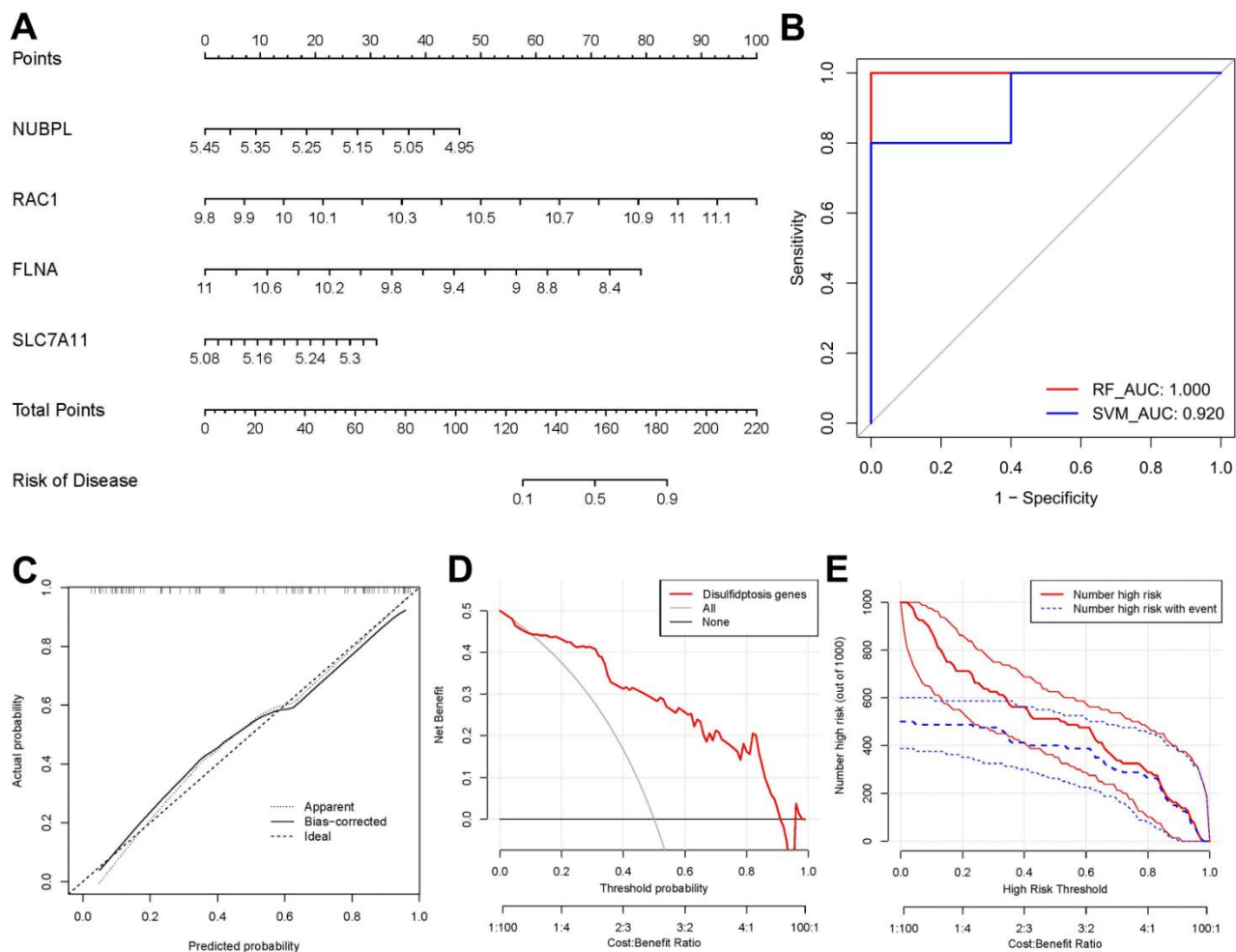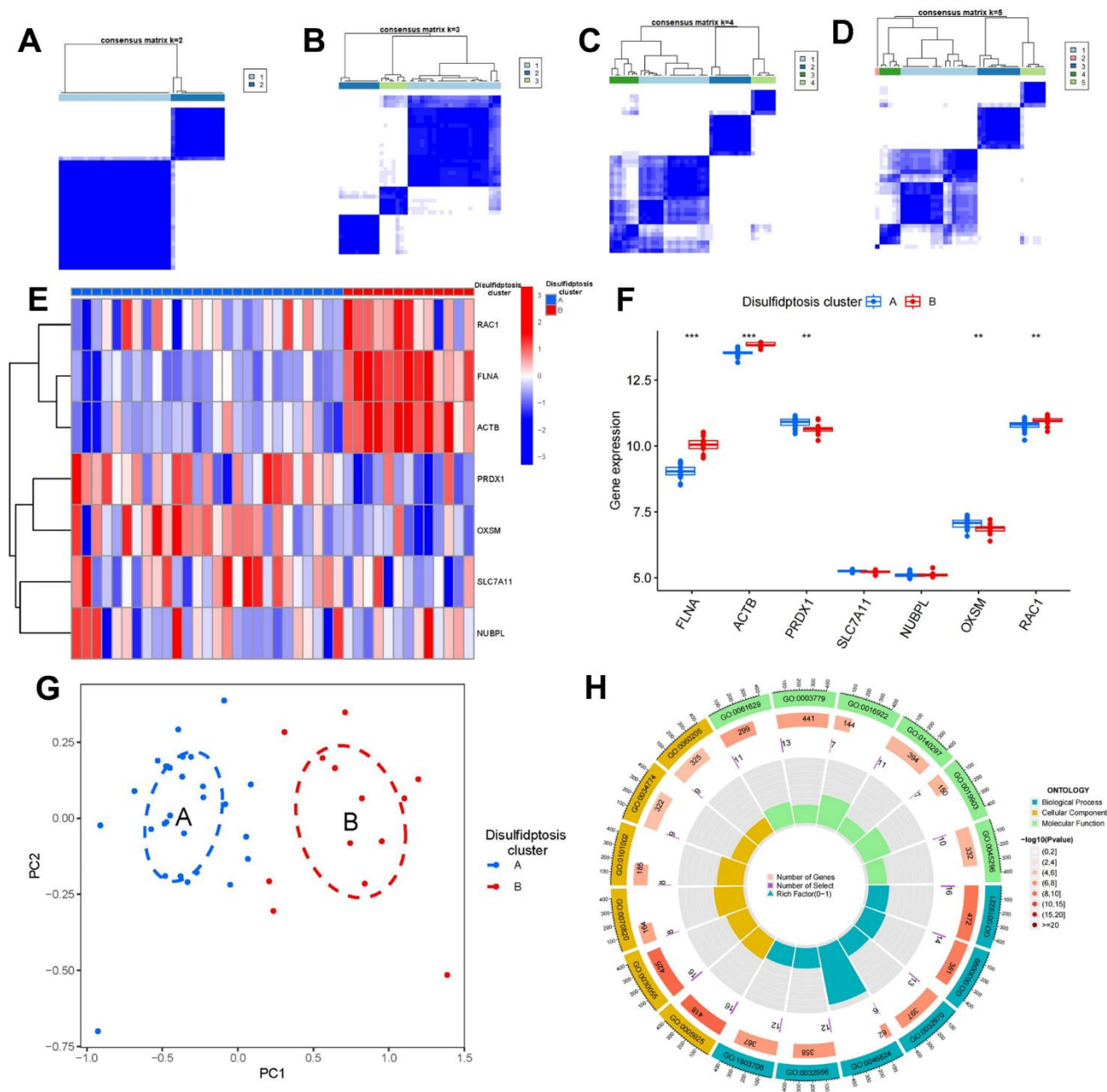

Figure 5. Establishment of the nomogram model. (**A**) A nomogram model was established based on four candidate disulfidptosis modulators. (**B**) The ROC result of our proposed signature in validation dataset GSE35956. (**C**) A calibration curve was utilised to evaluate the predictive accuracy of the nomogram model. (**D**) Decisions based on this nomogram model may be beneficial for clinical management of patients with OP. (**E**) A clinical impact curve was used to assess the clinical impact of the nomogram model.

Positive associations were noted among FLNA expression and several immune cell subsets (Figure 7A). Next, differences in immune cell infiltration were further explored between patients with high and low expression levels of FLNA. Remarkably, individuals with high FLNA expression displayed heightened immune cell infiltration in comparison to those with low FLNA expression (Figure 7B). Cluster B emerged to be more strongly correlated with OP, given its association with immature dendritic cells, monocytes, and T follicular helper cells, which are closely involved in osteoclast differentiation. Conversely, cluster A was associated with activated CD8$^+$ T cells and type 2 T helper cells (Figure 7C).

Figure 6. Consensus clustering of seven significant disulfidptosis modulators in OP. (**A–D**) Consensus matrices of seven significant disulfidptosis modulators for k = 2–5. (**E**) Expression heat map of seven significant disulfidptosis modulators in clusters A and B. (**F**) Differential expression box plots of seven significant disulfidptosis modulators in clusters A and B. (**G**) Principal component analysis of the expression profiles of seven significant disulfidptosis modulators showing substantial differences in transcriptomes between the two disulfidptosis patterns. (**H**) GO enrichment analysis was performed to explore potential mechanisms underlying the effects of 127 disulfidptosis-related DEGs on the occurrence and development of OP. **$P < 0.01$, ***$P < 0.001$.

Disulfidptosis gene cluster construction

To delineate disulfidptosis patterns, we employed a consensus clustering technique to categorize OP samples into distinct genetic subtypes according to 127 disulfidptosis-associated DEGs. The analysis unveiled two distinct disulfidptosis gene clusters, denoted as gene clusters A and B, which aligned with the disulfidptosis clusters previously identified (Figure 8A–8D). Expression profiles of the 127 disulfidptosis-related DEGs in gene clusters A and B are described in Figure 8E. Furthermore, the levels of immune cell infiltration and the gene expressions of the seven vital disulfidptosis regulators in gene clusters A and B were also similar to the disulfidptosis patterns (Figure 8F, 8G), validating the precision of the consensus clustering method. Notably, cluster B and gene cluster B showed higher disulfidptosis scores in comparison to cluster A and gene cluster A (Figure 8H, 8I).
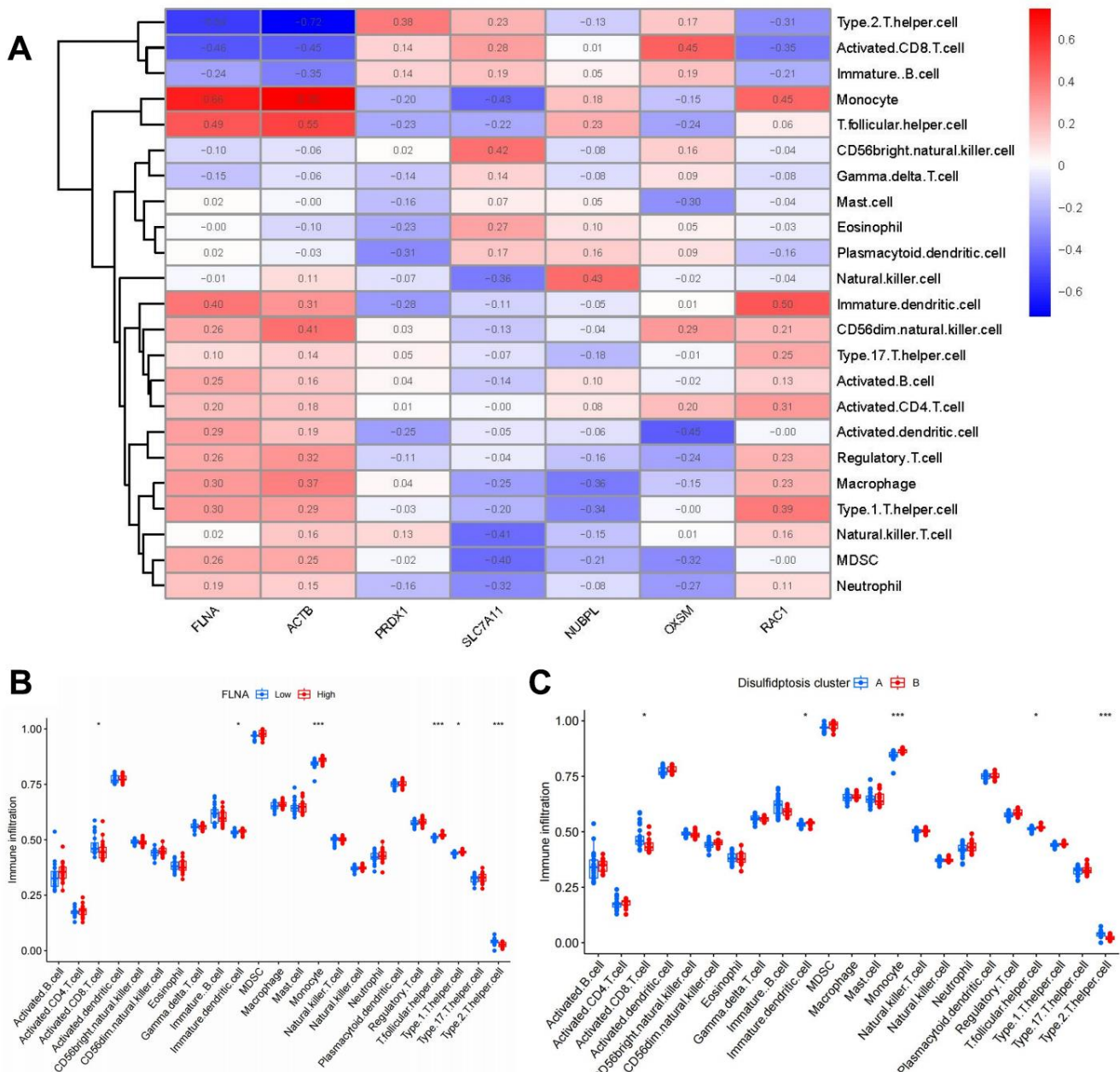

Figure 7. Single-sample gene set enrichment analysis. (**A**) Correlations between immune cell infiltration and seven significant disulfidptosis modulators. (**B**) Differences in abundance of infiltrating immune cells between high- and low-FLNA protein expression groups. (**C**) Differential immune cell infiltration between cluster A and cluster B. *$P < 0.05$, ***$P < 0.001$.

Role of disulfidptosis clusters in OP identification

The associations among disulfidptosis patterns, disulfidptosis scores, and disulfidptosis gene patterns are presented in Figure 9A. To explore the associations between OP and disulfidptosis patterns, we investigated correlations among disulfidptosis patterns and the expression levels of IL17RA, NFKB2, TP53, and RXRA, which are closely linked to osteoclast differentiation. Notably, higher expression levels of IL17RA, NFKB2, TP53, and RXRA were noted in cluster B and gene cluster B compared to cluster A and gene cluster A, suggesting a strong association of cluster B and gene cluster B with OP characterized by osteoclast differentiation (Figure 9B, 9C).

RNA-seq-based verification of important disulfidptosis regulators

After meticulous filtering, we identified two essential disulfidptosis modulators, PRDX1 and OXSM, which were illustrated via an expression heat map and volcano plot (Figure 10A, 10B). Notably, the disulfidptosis genes OXSM and PRDX1 exhibited significantly elevated expression levels in OP patients compared to controls (Figure 10C, 10D), validating the predictions generated from bioinformatics analyses.

DISCUSSION

OP is a prevalent musculoskeletal disorder marked by bone-related symptoms [26]. Previous studies have demonstrated that sulfide-related proteins can regulate the balance of bone metabolism in OP, indicating a potential involvement of disulfidptosis in the pathological process of OP [11–13]. However, it remains unclear whether disulfidptosis regulators play crucial roles in OP. The present study explored the roles of disulfidptosis regulators in OP pathology.

In this study, we utilized RF and SVM models to create a gene signature associated with disulfidptosis, employing the seven significant disulfidptosis regulators. The RF model operates as a learning
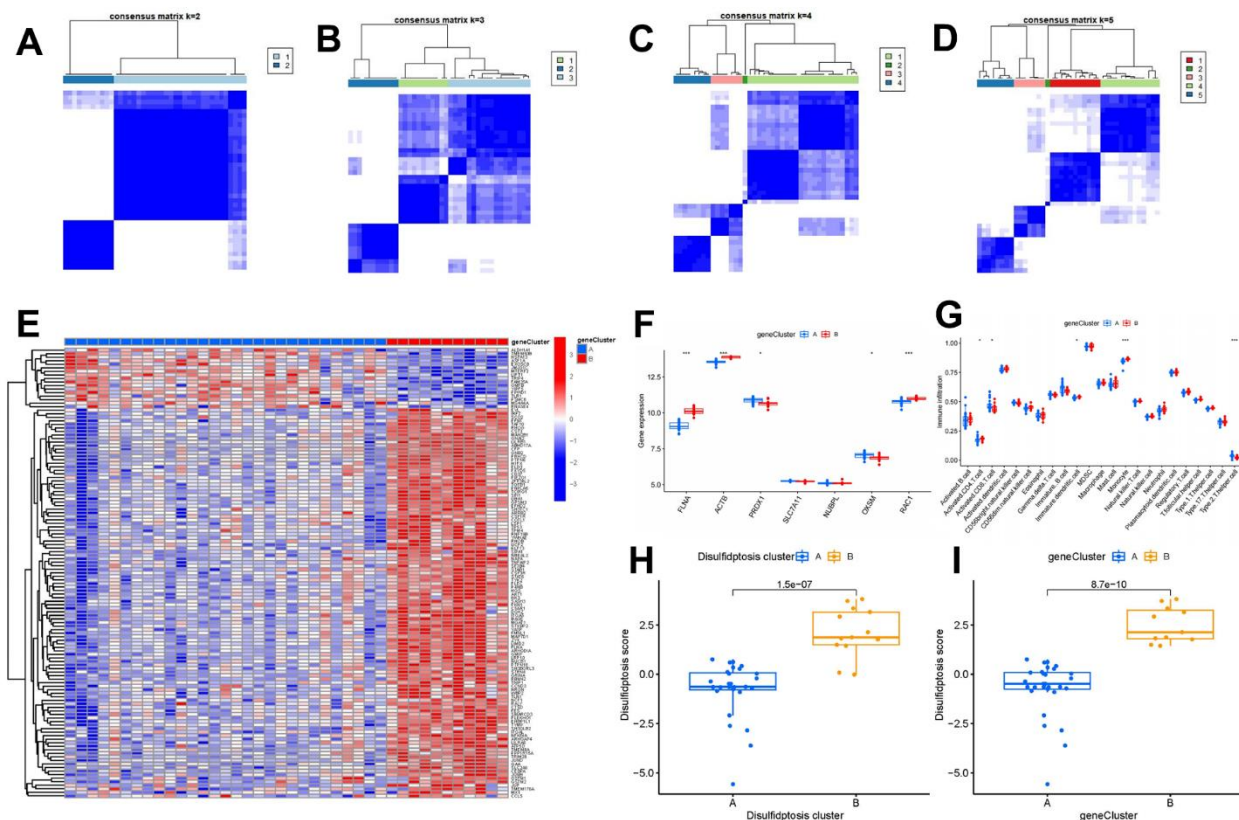

Figure 8. Consensus clustering of 127 disulfidptosis-associated DEGs in OP. (**A–D**) Consensus matrices of 127 disulfidptosis-associated DEGs for k = 2–5. (**E**) Expression heat map of 127 disulfidptosis-associated DEGs in gene clusters A and B. (**F**) Differential expression box plots of seven significant disulfidptosis modulators in gene clusters A and B. (**G**) Differential immune cell infiltration between gene clusters A and B. (**H**) Differences in disulfidptosis scores between cluster A and cluster B. (**I**) Differences in disulfidptosis scores between gene clusters A and B. *$P < 0.05$, ***$P < 0.001$.

algorithm by assembling independent decision trees derived from random samples. Each decision tree undergoes independent learning and prediction, with the final result being the average of all trees [27, 28]. On the other hand, the SVM model acts as a discriminative classifier, trained on labelled samples to classify test samples using the output of an optimal hyperplane [29]. In comparison to the SVM model, we observed that the RF model had higher AUC value and smaller residual, making it the most suitable testing model. Subsequently, the established RF model predicted the occurrence of OP, highlighting seven significant disulfidptosis regulators with differential expression between OP and control samples (namely, SLC7A11, FLNA, ACTB, PRDX1, NUBPL, OXSM, and RAC1) as potential diagnostic markers. Furthermore, we developed a nomogram model consisting of four potential disulfidptosis regulators (SLC7A11, FLNA, NUBPL, and RAC1) with significance scores > 6, based on DCA analysis of clinical benefits for OP patients.

Under circumstances of glucose deprivation, SLC7A11, also recognized as xCT, facilitates cystine intake and fosters disulfidptosis [10]. The upregulation of SLC7A11 *in vitro* has been demonstrated to significantly impede osteoblast differentiation of mesenchymal stem cells and dampen bone formation *in vivo* [30]. Additionally, SLC7A11 serves as an epigenetic cofactor that disrupts osteoclastogenesis [31]. OP is characterized by excessive osteoclast activity, and hindering osteoclast differentiation effectively shields against OP [32]. Previous study has revealed that NFATc1-induced upregulation of SLC7A11 triggers targetable sensitivity to thioredoxin reductase 1 (TXNRD1) inhibitors during osteoclastogenesis, potentially leading to the selective elimination of osteoclast precursors through intracellular cystine accumulation and subsequent disulfidptosis [33]. As a small GTPase, RAC1 (Ras-related C3 botulinum toxin substrate 1) is upregulated to activate disulfidptosis [10]. During osteoclast differentiation, RAC1 undergoes significant upregulation; its knockdown suppresses osteoclast differentiation and monocyte apoptosis [34]. PRDX1 (peroxiredoxin 1) is a known modulator of reactive oxygen species that regulates oxidative stress and BMP signalling-driven osteogenesis [35]. OXSM (mitochondrial 3-oxoacyl-ACP synthase) reportedly targets miR338-3p [36], which has important functions in regulating bone homeostasis in OP [37]. The present study confirmed that these genes—SLC7A11, RAC1, PRDX1 and OXSM—encoding disulfidptosis activators exhibited higher expression levels in OP samples, thereby activating disulfidptosis processes in OP.
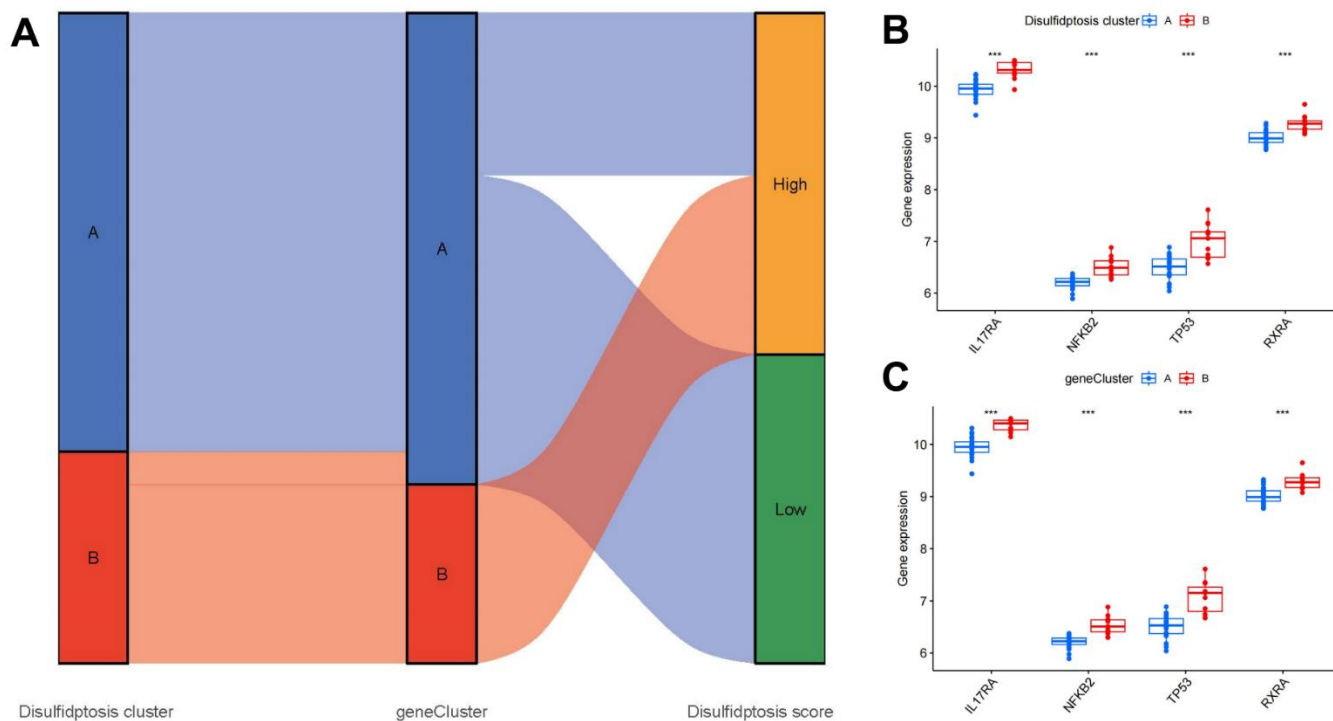

Figure 9. Roles of disulfidptosis patterns in distinguishing OP. (**A**) Sankey diagram showing relationships among disulfidptosis patterns, disulfidptosis gene patterns, and disulfidptosis scores. (**B**) Differential expression levels of osteoclast differentiation-related genes between cluster A and cluster B. (**C**) Differential expression levels of osteoclast differentiation-related genes between gene cluster A and gene cluster B. ***$P < 0.001$.

Actin cytoskeleton proteins exhibit high susceptibility to disulfide stress; abnormal disulfide bonding between actin cytoskeleton proteins has the potential to induce the collapse of the actin network and initiate disulfidptosis [10]. The actin cytoskeleton proteins, FLNA (filamin-A) and ACTB (actin), possess numerous cysteine sites that form disulfide bonds under conditions of glucose starvation; Alongside the NUBPL (nucleotide binding protein-like) factor associated with mitochondrial oxidative phosphorylation, these proteins act as disulfidptosis modulators, synergizing with glucose starvation to trigger disulfidptosis [10]. Previous research has shown that inactivation of ACTB blocks osteogenic differentiation and proliferation [38]. Evidence suggests that FLNA is involved in negatively regulating osteogenesis and positively modulating osteoclastogenesis [39]. Loss of NUBPL function triggers mitochondrial dysfunction [40], which could disrupt both bone formation and resorption [41]. Importantly, the present study confirmed that the disulfidptosis regulators ACTB, FLNA, and NUBPL exhibited lower expression levels in OP samples, thus influencing disulfidptosis processes in OP. In general, the seven potential disulfidptosis regulators screened in

this study may play crucial roles in OP onset and progression.

There is mounting evidence indicating the significance of monocyte osteoclastogenesis in the pathogenesis of OP [42]. Our study revealed that cluster A was associated with activated CD8+ T cell and type 2 T helper cell immunity, while cluster B was related to immature dendritic cell, monocyte, and T follicular helper cell immunity, which are closely associated with osteoclastogenesis; these findings suggest that cluster B is more closely associated with OP (Figure 7C). Monocytes play a pivotal role in maintaining immuno-logical homeostasis and preventing the onset of OP [43]. Monocytes differentiate into multinucleated osteoclasts, thereby regulating osteoclastogenesis in bone metabolism [44]. RXRA, IL17RA, NFKB2, and TP53 are closely linked to osteoclastogenesis. RXRA plays a pivotal role in the vitamin D pathway, which participates in regulating osteoclastogenesis in the context of bone homeostasis [45]. The immunological and skeletal systems share numerous regulatory components, including the IL-17a receptor (IL17RA); the deletion of IL17RA reduces the number of
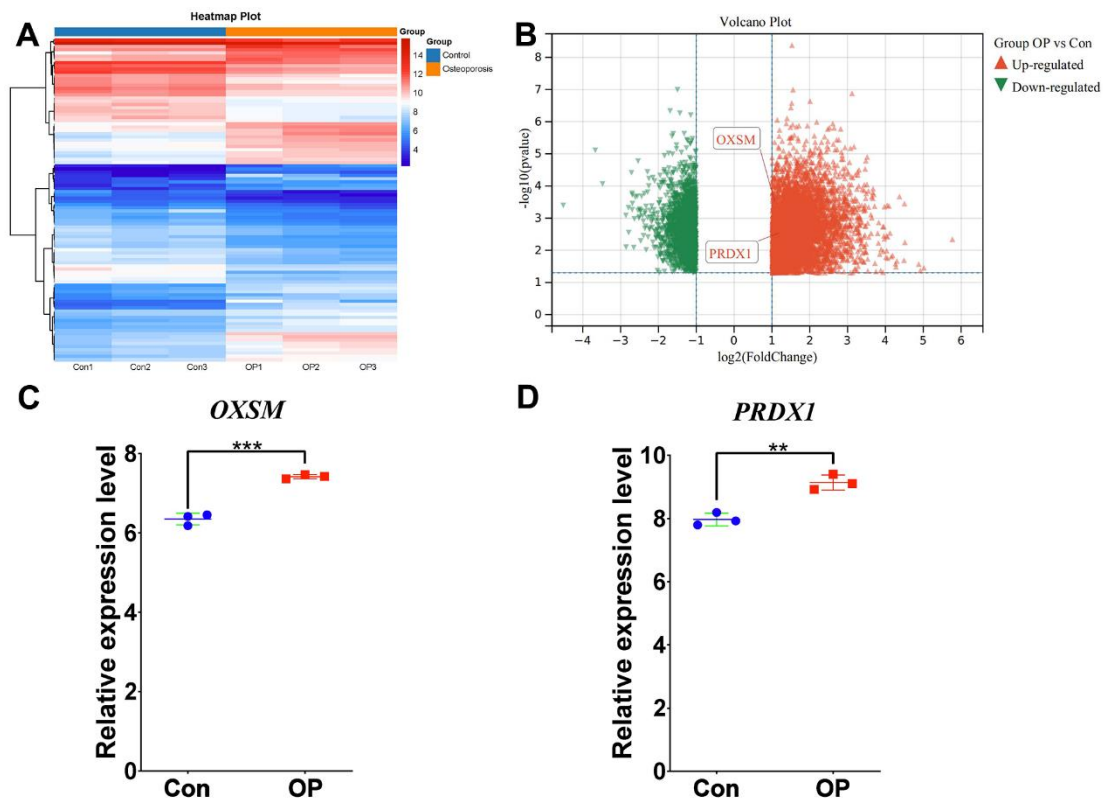

Figure 10. RNA-seq validation of significant disulfidptosis modulators. (**A**) Expression heat map and (**B**) volcano plot of vertebral bone tissues from patients with OP and controls, assessed by RNA-seq. (**C**) The disulfidptosis modulator OXSM exhibited increased expression levels in OP samples compared with controls. (**D**) The disulfidptosis modulator PRDX1 exhibited increased expression levels in OP samples compared with controls. All results are expressed as means ± standard deviations. **$P < 0.01$, ***$P < 0.001$.

osteoclast precursors and increases bone mass [46]. Osteoclastogenesis is negatively regulated by NFKB2 (p100); its blockade may prevent inflammation-mediated bone loss and bone deterioration in OP [47]. TP53 acts as a novel modulator of osteoblast-dependent osteo-clastogenesis [48]. In this study, we identified two disulfidptosis clusters (clusters A and B) using the seven significant disulfidptosis modulators; we also identified two different disulfidptosis gene clusters (gene clusters A and B) based on 127 disulfidptosis-associated DEGs. Cluster B was verified to have a close association with monocyte immunity and elevated levels in gene expressions of RXRA, IL17RA, NFKB2, and TP53, indicating its association with osteoclastogenesis. Additionally, PCA was employed to calculate the disulfidptosis scores, thereby enabling the quantification of disulfidptosis signatures. Notably, cluster B and gene cluster B demonstrated higher disulfidptosis scores compared to cluster A and gene cluster A.

The RNA-seq analysis revealed significantly increased expression levels of the disulfidptosis genes OXSM and PRDX1 in OP patients in comparison to controls (Figure 10). These findings validate the involvement of these disulfidptosis modulators in OP and bring insights on their role in OP etiology, offering support for the hypothesis that disulfidptosis regulators play a vital role in OP progression. These disulfidptosis modulators may represent promising therapeutic targets for efforts to balance bone formation and resorption in OP. To date, this study firstly establishes a diagnostic cluster and an immunological landscape associated with disulfidptosis in OP. However, the in-depth mechanisms by which disulfidptosis regulators influence OP-related pathways and immune microenvironment require further experimental validation.

CONCLUSIONS

In this study, we examined seven diagnostic disulfidptosis regulators and established a nomogram model with accurate prediction of OP incidence. By utilizing these vital disulfidptosis genes, two disulfidptosis signatures were identified, indicating that cluster B and gene cluster B may be more closely related to OP. To our knowledge, this research firstly elucidates a diagnostic cluster and an immunological landscape connected with disulfidptosis in OP.

AUTHOR CONTRIBUTIONS

Peng Zhang, Xiang Yu, De Liang, Jianchao Cui, Hui Ren, and Xiaobing Jiang contributed to the conceptualization and design. Peng Zhang, Bing Li, Honglin Chen, Zhilin Ge, and Qi Shang contributed to the methodology, formal analysis and validation. Peng Zhang, Bing Li and Honglin Chen contributed to data analysis, drafting and editing the manuscript. Peng Zhang, Bing Li and Honglin Chen contributed equally to this work. All authors read and approved the submitted manuscript.

ACKNOWLEDGMENTS

CONFLICTS OF INTEREST

The authors declare that they have no conflicts of interest.

ETHICAL STATEMENT AND CONSENT

This study protocol was approved by the Ethics Committee of the First Affiliated Hospital of Guangzhou University of Chinese Medicine with the approval number ZYYECR[2016]028. The informed consents were obtained from all patients who participated in this study.

FUNDING

REFERENCES

1. Arceo-Mendoza RM, Camacho PM. Postmenopausal Osteoporosis: Latest Guidelines. Endocrinol Metab Clin North Am. 2021; 50:167–78.
https://doi.org/10.1016/j.ecl.2021.03.009
PMID:34023036

2. Słupski W, Jawień P, Nowak B. Botanicals in Postmenopausal Osteoporosis. Nutrients. 2021; 13:1609.
https://doi.org/10.3390/nu13051609
PMID:34064936

3. Huidrom S, Beg MA, Masood T. Post-menopausal Osteoporosis and Probiotics. Curr Drug Targets. 2021; 22:816–22.
https://doi.org/10.2174/1389450121666201027124947 PMID:33109043

4. Reid IR. A broader strategy for osteoporosis interventions. Nat Rev Endocrinol. 2020; 16:333–9.
https://doi.org/10.1038/s41574-020-0339-7
PMID:32203407

5. Tian A, Jia H, Zhu S, Lu B, Li Y, Ma J, Ma X. Romosozumab versus Teriparatide for the Treatment of Postmenopausal Osteoporosis: A Systematic Review and Meta-analysis through a Grade Analysis of Evidence. Orthop Surg. 2021; 13:1941–50.
https://doi.org/10.1111/os.13136 PMID:34643048

6. Han J, Li L, Zhang C, Huang Q, Wang S, Li W, Zong J, Li L, Zhao Z, Zhang Z, Liu Z, Wang Q, Shi Y. Eucommia, Cuscuta, and Drynaria Extracts Ameliorate Glucocorticoid-Induced Osteoporosis by Inhibiting Osteoclastogenesis Through PI3K/Akt Pathway. Front Pharmacol. 2022; 12:772944.
https://doi.org/10.3389/fphar.2021.772944
PMID:35185535

7. McNeil MA, Merriam SB. Menopause. Ann Intern Med. 2021; 174:ITC97–TC112.
https://doi.org/10.7326/AITC202107200
PMID:34251902

8. Si L, Winzenberg TM, Jiang Q, Chen M, Palmer AJ. Projection of osteoporosis-related fractures and costs in China: 2010-2050. Osteoporos Int. 2015; 26:1929–37.
https://doi.org/10.1007/s00198-015-3093-2
PMID:25761729

9. Yin L, Zhu X, Novák P, Zhou L, Gao L, Yang M, Zhao G, Yin K. The epitranscriptome of long noncoding RNAs in metabolic diseases. Clin Chim Acta. 2021; 515:80–9.
https://doi.org/10.1016/j.cca.2021.01.001
PMID:33422492

10. Liu X, Nie L, Zhang Y, Yan Y, Wang C, Colic M, Olszewski K, Horbath A, Chen X, Lei G, Mao C, Wu S, Zhuang L, et al. Actin cytoskeleton vulnerability to disulfide stress mediates disulfidptosis. Nat Cell Biol. 2023; 25:404–14.
https://doi.org/10.1038/s41556-023-01091-2
PMID:36747082

11. Cai X, Yi X, Zhang Y, Zhang D, Zhi L, Liu H. Genetic susceptibility of postmenopausal osteoporosis on sulfide quinone reductase-like gene. Osteoporos Int. 2018; 29:2041–7.
https://doi.org/10.1007/s00198-018-4575-9
PMID:29855663

12. Jin HS, Kim J, Park S, Park E, Kim BY, Choi VN, Yoo YH, Kim BT, Jeong SY. Association of the I264T variant in the sulfide quinone reductase-like (SQRDL) gene with osteoporosis in Korean postmenopausal women. PLoS One. 2015; 10:e0135285.
https://doi.org/10.1371/journal.pone.0135285
PMID:26258864

13. Yang J, Tang R, Yi J, Chen Y, Li X, Yu T, Fei J. Diallyl disulfide alleviates inflammatory osteolysis by suppressing osteoclastogenesis via NF-κB-NFATc1 signal pathway. FASEB J. 2019; 33:7261–73.
https://doi.org/10.1096/fj.201802172R
PMID:30857415

14. Pan C, Zhang C, Lin Z, Liang Z, Cui Y, Shang Z, Wei Y, Chen F. Disulfidptosis-related Protein RPN1 May be a Novel Anti-osteoporosis Target of Kaempferol. Comb Chem High Throughput Screen. 2024. [Epub ahead of print].
https://doi.org/10.2174/01138620732736552312130 70619 PMID:38213143

15. Zhou Y, Gao Y, Xu C, Shen H, Tian Q, Deng HW. A novel approach for correction of crosstalk effects in pathway analysis and its application in osteoporosis research. Sci Rep. 2018; 8:668.
https://doi.org/10.1038/s41598-018-19196-2
PMID:29330445

16. Dai B, Sun F, Cai X, Li C, Liu H, Shang Y. Significance of RNA N6-Methyladenosine Regulators in the Diagnosis and Subtype Classification of Childhood Asthma Using the Gene Expression Omnibus Database. Front Genet. 2021; 12:634162.
https://doi.org/10.3389/fgene.2021.634162
PMID:33763115

17. Hu Y, Han J, Ding S, Liu S, Wang H. Identification of ferroptosis-associated biomarkers for the potential diagnosis and treatment of postmenopausal osteoporosis. Front Endocrinol (Lausanne). 2022; 13:986384.
https://doi.org/10.3389/fendo.2022.986384
PMID:36105394

18. Zhang P, Chen H, Zhang Y, Liu Y, Zhu G, Zhao W, Shang Q, He J, Zhou Z, Shen G, Yu X, Zhang Z, Chen G, et al. Dry and wet experiments reveal diagnostic clustering and immune landscapes of cuproptosis patterns in patients with ankylosing spondylitis. Int Immunopharmacol. 2024; 127:111326.
https://doi.org/10.1016/j.intimp.2023.111326
PMID:38091828

19. Ritchie ME, Phipson B, Wu D, Hu Y, Law CW, Shi W,

Smyth GK. limma powers differential expression analyses for RNA-sequencing and microarray studies. Nucleic Acids Res. 2015; 43:e47. https://doi.org/10.1093/nar/gkv007 PMID:25605792

20. Bao X, Shi R, Zhao T, Wang Y. Mast cell-based molecular subtypes and signature associated with clinical outcome in early-stage lung adenocarcinoma. Mol Oncol. 2020; 14:917–32. https://doi.org/10.1002/1878-0261.12670 PMID:32175651

21. Benisch P, Schilling T, Klein-Hitpass L, Frey SP, Seefried L, Raaijmakers N, Krug M, Regensburger M, Zeck S, Schinke T, Amling M, Ebert R, Jakob F. The transcriptional profile of mesenchymal stem cell populations in primary osteoporosis is distinct and shows overexpression of osteogenic inhibitors. PLoS One. 2012; 7:e45142. https://doi.org/10.1371/journal.pone.0045142 PMID:23028809

22. Wilkerson MD, Hayes DN. ConsensusClusterPlus: a class discovery tool with confidence assessments and item tracking. Bioinformatics. 2010; 26:1572–3. https://doi.org/10.1093/bioinformatics/btq170 PMID:20427518

23. Denny P, Feuermann M, Hill DP, Lovering RC, Plun-Favreau H, Roncaglia P. Exploring autophagy with Gene Ontology. Autophagy. 2018; 14:419–36. https://doi.org/10.1080/15548627.2017.1415189 PMID:29455577

24. Zhang B, Wu Q, Li B, Wang D, Wang L, Zhou YL. m6A regulator-mediated methylation modification patterns and tumor microenvironment infiltration characterization in gastric cancer. Mol Cancer. 2020; 19:53. https://doi.org/10.1186/s12943-020-01170-0 PMID:32164750

25. Zhang N, Zhao YD, Wang XM. CXCL10 an important chemokine associated with cytokine storm in COVID-19 infected patients. Eur Rev Med Pharmacol Sci. 2020; 24:7497–505. https://doi.org/10.26355/eurrev_202007_21922 PMID:32706090

26. Eastell R, Szulc P. Use of bone turnover markers in postmenopausal osteoporosis. Lancet Diabetes Endocrinol. 2017; 5:908–23. https://doi.org/10.1016/S2213-8587(17)30184-5 PMID:28689768

27. Albaradei S, Thafar M, Alsaedi A, Van Neste C, Gojobori T, Essack M, Gao X. Machine learning and deep learning methods that use omics data for metastasis prediction. Comput Struct Biotechnol J. 2021; 19:5008–18. https://doi.org/10.1016/j.csbj.2021.09.001 PMID:34589181

28. Buckley SJ, Harvey RJ. Lessons Learnt From Using the Machine Learning Random Forest Algorithm to Predict Virulence in Streptococcus pyogenes. Front Cell Infect Microbiol. 2021; 11:809560. https://doi.org/10.3389/fcimb.2021.809560 PMID:35004362

29. Satake H, Osugi T, Shiraishi A. Impact of Machine Learning-Associated Research Strategies on the Identification of Peptide-Receptor Interactions in the Post-Omics Era. Neuroendocrinology. 2023; 113:251–61. https://doi.org/10.1159/000518572 PMID:34348315

30. Jin C, Zhang P, Zhang M, Zhang X, Lv L, Liu H, Liu Y, Zhou Y. Inhibition of SLC7A11 by Sulfasalazine Enhances Osteogenic Differentiation of Mesenchymal Stem Cells by Modulating BMP2/4 Expression and Suppresses Bone Loss in Ovariectomized Mice. J Bone Miner Res. 2017; 32:508–21. https://doi.org/10.1002/jbmr.3009 PMID:27696501

31. Lee S, Kim HS, Kim MJ, Min KY, Choi WS, You JS. Glutamine metabolite α-ketoglutarate acts as an epigenetic co-factor to interfere with osteoclast differentiation. Bone. 2021; 145:115836. https://doi.org/10.1016/j.bone.2020.115836 PMID:33383217

32. Reid IR, Billington EO. Drug therapy for osteoporosis in older adults. Lancet. 2022; 399:1080–92. https://doi.org/10.1016/S0140-6736(21)02646-5 PMID:35279261

33. Zhong Z, Zhang C, Ni S, Ma M, Zhang X, Sang W, Lv T, Qian Z, Yi C, Yu B. NFATc1-mediated expression of SLC7A11 drives sensitivity to TXNRD1 inhibitors in osteoclast precursors. Redox Biol. 2023; 63:102711. https://doi.org/10.1016/j.redox.2023.102711 PMID:37148740

34. Zhang L, Li X, Wan C, Da W, Zhang J, Fan L, Fu Q, Xing S, Wang Y. Bioinformatics analysis identification of AKT3 and RAC1 as key genes in postmenopausal osteoporosis. Exp Ther Med. 2022; 24:656. https://doi.org/10.3892/etm.2022.11592 PMID:36168425

35. Kumar Y, Biswas T, Thacker G, Kanaujiya JK, Kumar S, Shukla A, Khan K, Sanyal S, Chattopadhyay N, Bandyopadhyay A, Trivedi AK. BMP signaling-driven osteogenesis is critically dependent on Prdx-1 expression-mediated maintenance of chondrocyte prehypetrophy. Free Radic Biol Med. 2018; 118:1–12. https://doi.org/10.1016/j.freeradbiomed.2018.02.016 PMID:29452246

36. Wang WY, Lu WC. Reduced Expression of hsa-miR-338-3p Contributes to the Development of Glioma Cells by Targeting Mitochondrial 3-Oxoacyl-ACP Synthase (OXSM) in Glioblastoma (GBM). Onco Targets Ther. 2020; 13:9513–23.
https://doi.org/10.2147/OTT.S262873
PMID:33061435

37. Tong J, Zhang M, Li X, Ren G. MicroRNA-338-3p regulates age-associated osteoporosis via targeting PCSK5. Mol Med Rep. 2021; 23:136.
https://doi.org/10.3892/mmr.2020.11775
PMID:33313955

38. Wang J, Yang H, Ma X, Liu J, Li L, Chen L, Wei F. LRP6/filamentous-actin signaling facilitates osteogenic commitment in mechanically induced periodontal ligament stem cells. Cell Mol Biol Lett. 2023; 28:7.
https://doi.org/10.1186/s11658-023-00420-5
PMID:36694134

39. Yang C, Yang P, Liu P, Wang H, Ke E, Li K, Yan H. Targeting Filamin A alleviates ovariectomy-induced bone loss in mice via the WNT/β-catenin signaling pathway. Cell Signal. 2022; 90:110191.
https://doi.org/10.1016/j.cellsig.2021.110191
PMID:34774991

40. Eis PS, Huang N, Langston JW, Hatchwell E, Schüle B. Loss-of-Function NUBPL Mutation May Link Parkinson's Disease to Recessive Complex I Deficiency. Front Neurol. 2020; 11:555961.
https://doi.org/10.3389/fneur.2020.555961
PMID:33224084

41. Zhou Q, Chen W, Gu C, Liu H, Hu X, Deng L, He W, Xu Y, Zhu X, Yang H, Chen X, He F, Liu T. Selenium-modified bone cement promotes osteoporotic bone defect repair in ovariectomized rats by restoring GPx1-mediated mitochondrial antioxidant functions. Regen Biomater. 2023; 10:rbad011.
https://doi.org/10.1093/rb/rbad011 PMID:36852397

42. Huang H, Ma S, Xing X, Su X, Xu X, Tang Q, Gao X, Yang J, Li M, Liang C, Wu Y, Liao L, Tian W. Muscle-derived extracellular vesicles improve disuse-induced osteoporosis by rebalancing bone formation and bone resorption. Acta Biomater. 2023; 157:609–24.
https://doi.org/10.1016/j.actbio.2022.12.019
PMID:36526242

43. Li H, Zhang X, Zhang Q, Zhang Q, Zhu X, Xie T, Wang S. The relationship between the monocyte-to-lymphocyte ratio and osteoporosis in postmenopausal females with T2DM: A retrospective study in Chinese population. Front Endocrinol (Lausanne). 2023; 14:1112534.
https://doi.org/10.3389/fendo.2023.1112534
PMID:36891058

44. Vuoti E, Lehenkari P, Tuukkanen J, Glumoff V, Kylmäoja E. Osteoclastogenesis of human peripheral blood, bone marrow, and cord blood monocytes. Sci Rep. 2023; 13:3763.
https://doi.org/10.1038/s41598-023-30701-0
PMID:36882450

45. Gu J, Zhang X, Zhang C, Li Y, Bian J, Liu X, Yuan Y, Zou H, Tong X, Liu Z. Galectin-3 Contributes to the Inhibitory Effect of Iα,25-(OH)2D3 on Osteoclastogenesis. Int J Mol Sci. 2021; 22:13334.
https://doi.org/10.3390/ijms222413334
PMID:34948130

46. Roberts JL, Mella-Velazquez G, Dar HY, Liu G, Drissi H. Deletion of IL-17ra in osteoclast precursors increases bone mass by decreasing osteoclast precursor abundance. Bone. 2022; 157:116310.
https://doi.org/10.1016/j.bone.2021.116310
PMID:34973492

47. Yao Z, Xing L, Boyce BF. NF-kappaB p100 limits TNF-induced bone resorption in mice by a TRAF3-dependent mechanism. J Clin Invest. 2009; 119:3024–34.
https://doi.org/10.1172/JCI38716 PMID:19770515

48. Wang X, Kua HY, Hu Y, Guo K, Zeng Q, Wu Q, Ng HH, Karsenty G, de Crombrugghe B, Yeh J, Li B. p53 functions as a negative regulator of osteoblastogenesis, osteoblast-dependent osteoclastogenesis, and bone remodeling. J Cell Biol. 2006; 172:115–25.
https://doi.org/10.1083/jcb.200507106
PMID:16380437

Supplementary Table 1. The detailed information of GO enrichment analysis in Figure 2J.

ONTOLOGY	ID	Description	p-value	p.adjust
BP	GO:0070527	platelet aggregation	1.04E-06	0.000432302
BP	GO:0034109	homotypic cell-cell adhesion	2.72E-06	0.000432302
BP	GO:0007596	blood coagulation	3.46E-06	0.000432302
BP	GO:0007599	hemostasis	3.66E-06	0.000432302
BP	GO:0050817	coagulation	3.71E-06	0.000432302
BP	GO:0051668	localization within membrane	1.67E-05	0.001535649
BP	GO:0030168	platelet activation	1.84E-05	0.001535649
BP	GO:0001894	tissue homeostasis	5.99E-05	0.004364239
BP	GO:0034329	cell junction assembly	7.16E-05	0.004635332
BP	GO:1900026	positive regulation of substrate adhesion-dependent cell spreading	7.98E-05	0.004649556
CC	GO:0098978	glutamatergic synapse	0.000182539	0.004467089
CC	GO:0005925	focal adhesion	0.000283152	0.004467089
CC	GO:0005924	cell-substrate adherens junction	0.000289373	0.004467089
CC	GO:0030055	cell-substrate junction	0.000297806	0.004467089
CC	GO:0042470	melanosome	0.00059076	0.005301481
CC	GO:0048770	pigment granule	0.00059076	0.005301481
CC	GO:0005884	actin filament	0.000647536	0.005301481
CC	GO:0030863	cortical cytoskeleton	0.000706864	0.005301481
CC	GO:0044448	cell cortex part	0.001763774	0.011758497
CC	GO:0036464	cytoplasmic ribonucleoprotein granule	0.002332005	0.013992032
MF	GO:0030957	Tat protein binding	0.003949442	0.043175984
MF	GO:0004312	fatty acid synthase activity	0.00434365	0.043175984
MF	GO:0031996	thioesterase binding	0.00434365	0.043175984
MF	GO:0099186	structural constituent of postsynapse	0.00434365	0.043175984
MF	GO:0005313	L-glutamate transmembrane transporter activity	0.005525471	0.043175984
MF	GO:0015172	acidic amino acid transmembrane transporter activity	0.005525471	0.043175984
MF	GO:0050998	nitric-oxide synthase binding	0.005525471	0.043175984
MF	GO:0017160	Ral GTPase binding	0.005919144	0.043175984
MF	GO:0072349	modified amino acid transmembrane transporter activity	0.005919144	0.043175984
MF	GO:0098918	structural constituent of synapse	0.00670609	0.043175984

Supplementary Table 2. The detailed information of KEGG enrichment analysis in Figure 2K.

Term	p-value	p.adjust
Focal adhesion	3.40E-05	0.001225119
Proteoglycans in cancer	3.60E-05	0.001225119
Salmonella infection	6.43E-05	0.00145771
Viral myocarditis	1.84E-04	0.003129081
Adherens junction	2.58E-04	0.003438715
Bacterial invasion of epithelial cells	3.03E-04	0.003438715
Leukocyte transendothelial migration	6.64E-04	0.006448343
Yersinia infection	9.56E-04	0.007437068
Fluid shear stress and atherosclerosis	9.84E-04	0.007437068
Phagosome	0.00117522	0.007991495
Tight junction	0.001449643	0.008961432
Neutrophil extracellular trap formation	0.001808145	0.010246156
Pathogenic Escherichia coli infection	0.001962254	0.010264096
Rap1 signaling pathway	0.002225638	0.01081024
Regulation of actin cytoskeleton	0.002395654	0.010860298
Shigellosis	0.00303791	0.012911117
MAPK signaling pathway	0.004307241	0.017228962
Fatty acid biosynthesis	0.006283878	0.023369719
Amyotrophic lateral sclerosis	0.006529775	0.023369719
Ferroptosis	0.014264049	0.048497766

Supplementary Table 3. The detailed information of GO enrichment analysis in Figure 6H.

ONTOLOGY	ID	Description	p-value	p.adjust
BP	GO:0019221	cytokine-mediated signaling pathway	4.02E-08	0.000115189
BP	GO:0030099	myeloid cell differentiation	1.13E-07	0.000162544
BP	GO:0032970	regulation of actin filament-based process	1.21E-06	0.00116027
BP	GO:0046824	positive regulation of nucleocytoplasmic transport	2.42E-06	0.001442425
BP	GO:0032956	regulation of actin cytoskeleton organization	2.52E-06	0.001442425
BP	GO:1903706	regulation of hemopoiesis	3.25E-06	0.001542839
CC	GO:0005925	focal adhesion	7.45E-09	1.22E-06
CC	GO:0030055	cell-substrate junction	9.42E-09	1.22E-06
CC	GO:0070820	tertiary granule	8.85E-06	0.000763914
CC	GO:0101002	ficolin-1-rich granule	2.12E-05	0.001374605
CC	GO:0034774	secretory granule lumen	0.000190749	0.007136597
CC	GO:0060205	cytoplasmic vesicle lumen	0.000204362	0.007136597
MF	GO:0061629	RNA polymerase II-specific DNA-binding transcription factor binding	4.26E-06	0.001141206
MF	GO:0003779	actin binding	6.29E-06	0.001141206
MF	GO:0016922	nuclear receptor binding	4.47E-05	0.003936513
MF	GO:0140297	DNA-binding transcription factor binding	5.51E-05	0.003936513
MF	GO:0019903	protein phosphatase binding	5.80E-05	0.003936513
MF	GO:0045296	cadherin binding	6.51E-05	0.003936513